

Precision measurements and calculations in the B II spectrum: Wavelengths, isotope shifts, and oscillator strengths

Ulf Litzén and Torgil Zethson

Department of Physics, Lund University, P.O. Box 118, S-221 00 Lund, Sweden

Per Jönsson

Department of Physics, Lund Institute of Technology, P.O. Box 118, S-221 00 Lund, Sweden

Jörg Kasten and Rainer Kling

Institute for Atomic and Molecular Physics, Plasma Physics Division, Callinstrasse 38, D-3000 Hannover, Germany

Françoise Launay

Observatoire de Paris, Section de Meudon, DAMAp and CNRS-URA 812, 5 Place Jules Janssen, F-92195 Meudon Cedex, France

(Received 2 December 1997)

Recordings of boron spectra with high-dispersion grating spectroscopy and Fourier transform spectroscopy have provided high-precision wavelengths and transition isotope shifts for all LS -allowed transitions involving the $2s^2$, $2s2p$, and $2p^2$ configurations in the spectrum of singly ionized boron B II. Large-scale calculations of the same quantities have been performed with the multiconfiguration Hartree-Fock method. There is agreement between the measurements and the calculations within the narrow error limits for all the lines. The calculations also yielded oscillator strengths and hyperfine-structure constants for the same transitions.

[S1050-2947(98)05804-1]

PACS number(s): 32.30.Jc, 31.30.Gs, 32.10.Bi, 32.70.Cs

I. INTRODUCTION

Astronomical observations of the relative abundance of the two boron isotopes ^{10}B and ^{11}B are expected to provide information about the cosmic production of the light elements. The observed abundance ratio in the solar system is about 4, in contrast, e.g., to the value 2.5, derived from a proposed production process through nuclear spallation reactions (see, e.g., Ref. [1] and references therein).

It is difficult, however, to measure this ratio in astronomical objects. Due to the small isotope shift the spectral lines from the two isotopes cannot be resolved, but the abundance ratio has to be determined through curve fitting of boron line profiles to the observed stellar feature. Due to the low cosmic abundance the stellar boron lines are weak and may be severely perturbed by adjacent lines from more abundant elements. An accurate value for the isotope shift, to be used as a fixed parameter in the curve-fitting procedure, is therefore crucial for a determination of the isotopic abundance ratio. In addition to the isotope shift, i.e., the distance between the line components, also accurate absolute wavelengths are needed for boron abundance analysis in stellar spectra [2].

Laboratory measurements of transition isotope shifts (TISs) and absolute wavelengths of the B I resonance lines are available [3], but the ionization balance in the relevant astronomical objects implies that a better signal-to-noise ratio could be achieved by observing the B II resonance line at 1362 Å. To our knowledge, the TIS in this line has not been measured previously in the laboratory. Instead, it has been calculated to be 13.3 mÅ, with an estimated uncertainty of less than 1% [4]. A recent analysis of the 1362-Å line profile observed in Hubble spectra of the interstellar medium [1] indicated a TIS of 13.7 ± 3.5 mÅ.

The present investigation was performed in order to provide accurate experimental values for the absolute wavelength and the TIS of the B II resonance line. The measurements also comprise wavelengths and isotope shifts of other transitions involving the $2s2p$ and $2p^2$ configurations in B II. The measurements are supported by accurate multiconfiguration Hartree-Fock calculations, which, in addition to the isotope shifts, also provide values of hyperfine constants and oscillator strengths.

II. EXPERIMENT

The boron spectrum was emitted from a hollow cathode source, described by Danzmann *et al.* [5]. The cathode consisted of a tube of boron carbide (B_4C) covering the inside of a copper tube, which was inserted into the water-cooled cathode part of the light source. To provide standard lines for the wavelength calibration, a compound cathode was used for some of the recordings. In this case only part of the length of the cathode consisted of B_4C , while the rest was made from pure iron. The inner diameter of the cathode tube was 8 mm.

The discharge in this source can be run at stable conditions over a wide current range. In the present experiment currents from 150 mA to 3 A were used. The lowest current was used in order to reduce the Doppler linewidth in the efforts to resolve the isotope structure of the resonance line, while the higher currents were used to improve the signal-to-noise (S/N) ratio for the rest of the lines. A flow of neon at 1 Torr or a helium-neon mixture at 3–5 Torr was used as the carrier gas. Also in this case the purpose of varying the conditions was to reduce the linewidth and to increase the S/N ratio.

A. Grating measurements

The B II lines below 1750 Å were recorded with the Meudon Observatory Eagle mounting vacuum ultraviolet 10-m spectrograph. The instrument is equipped with a concave ($R=10.685$ m), 3600-lines/mm, 30-cm-diam, Jobin-Yvon holographic grating coated with Al + MgF₂. This grating gives a plate factor of about 0.26 Å/mm in the first order and a resolving limit of 8 mÅ throughout the whole range of observation with a slit width of 30 μm and Kodak short wavelength radiation (SWR) plates.

1. Photographic recording

In the present experiment Fe II lines around 1360 Å emitted by the B₄ C/Fe hollow cathode at 150 mA and recorded on Kodak SWR plates were found to have a width on the plate of 30 μm, corresponding to 8 mÅ, i.e., the maximum attainable resolution was achieved. Evidently, the Doppler width of the Fe II lines was negligible. The B I lines at 1379 Å were somewhat wider, 35–40 μm. This is most probably due to the Doppler width of the light atoms being larger by a factor 2.3 compared to iron:

$$\frac{\delta\lambda_D}{\lambda} = \frac{\delta\sigma_D}{\sigma} = 7.16 \times 10^{-7} \sqrt{\frac{T}{M}}$$

It should thus in principle be possible to resolve the predicted isotope splitting of 13.3 mÅ at the B II 1362-Å resonance line, corresponding to 51 μm on the plate.

Several exposures of the region around the B II 1362-Å resonance line were made with different currents, pressures, and exposure times. The line was found to be asymmetric, but it was impossible to resolve the two isotope components. This does not necessarily imply that the isotope interval is smaller than the predicted 13.3 mÅ. A careful examination of the different exposures indicates that the intensity ratio of the two Doppler-broadened components, equal to the ¹¹B:¹⁰B abundance ratio 4:1, together with the nonlinear photographic response function and the high contrast of the SWR emulsion causes a problem. At a short exposure the line is symmetric, suggesting that only the ¹¹B component is detected. As the exposure time is increased, the blackening of this component increases, and before the ¹⁰B component appears above the background level, the width of the ¹¹B line has grown to such an extent that the weak line only appears as an asymmetry in the long-wavelength wing of the strong one.

Attempts to determine the isotope shift by means of curve fitting to the digitized profile of the photographic blackening failed, as the photographic nonlinearity affects both the line shapes, the linewidths, and the recorded intensity ratio. Exposures with Ilford Q plates, supposed to have a lower contrast, did not improve the situation.

Also the $2s2p\ ^3P - 2p^2\ ^3P$ multiplet at 1624 Å was recorded photographically. An isotope structure was observed for all six lines of the multiplet, but also in this case the structure was not fully resolved. The distance between the components, however, was found to be larger than for the resonance line and curve fitting routines with different sets of free parameters provided consistent results for the isotope splitting.

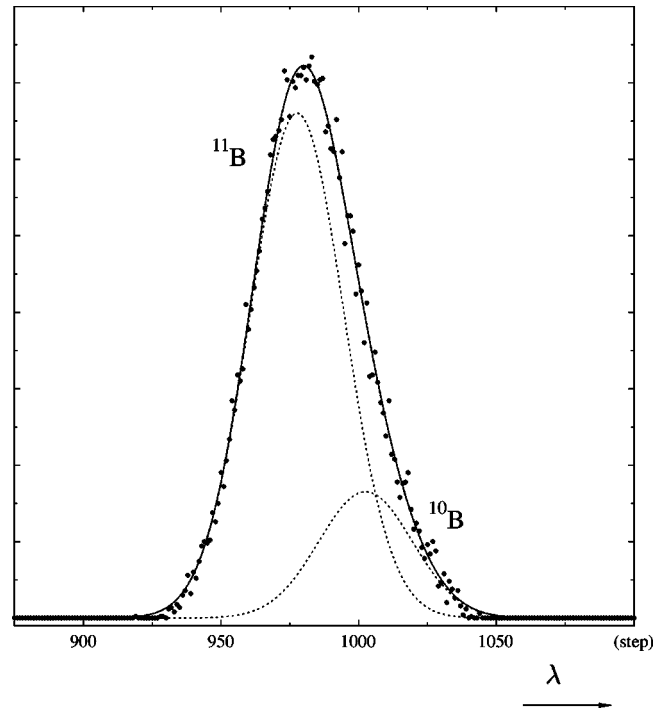


FIG. 1. Photoelectric scan of the B II resonance line at 1362 Å. The figure shows the recorded intensity (dots), the fitted isotope components (dotted lines), and the sum of the fitted components (solid line). The scale is given as the number of steps, where each step of 2 μm corresponds to 0.5 mÅ. The wavelength is increasing to the right.

2. Photoelectric recording

In order to overcome the difficulties concerning the isotope shift of the 1362-Å line, caused by the nonlinear photographic response, the photoelectric recording facility at the Meudon spectrograph was used. In this recording mode the plate holder is replaced by a device consisting of a photomultiplier tube (Hamamatsu R1459) behind an exit slit, which can be translated along the focal curve by means of a stepping motor and a precision screw.

An exit slit width of 30 μm, equal to the entrance slit of the spectrograph, was used in this experiment. The step length was 2 μm, with an integration time of 300 ms per step. The B₄C hollow cathode was run at 200 mA and 2 Torr of neon.

A scan over the B I lines at 1379 Å showed a somewhat larger line width, about 60 μm full width at half maximum, compared to the photographic recording. Also in this case the 1362-Å B II line was recorded as an unresolved, asymmetric feature; see Fig. 1. The great advantage compared to the photographic recording is the fact that the linear response of the photomultiplier enables an accurate determination of the two components by means of curve fitting.

B. FTS measurements

The boron spectrum in the wavelength region above 1750 Å was recorded with the Fourier transform spectrometer (FTS) at the Physics Department, Lund University. This instrument, a Chelsea Instruments type FT500, is specially designed for the UV region [6], with the lower wavelength limit set by the transmission of the silica beam splitter.

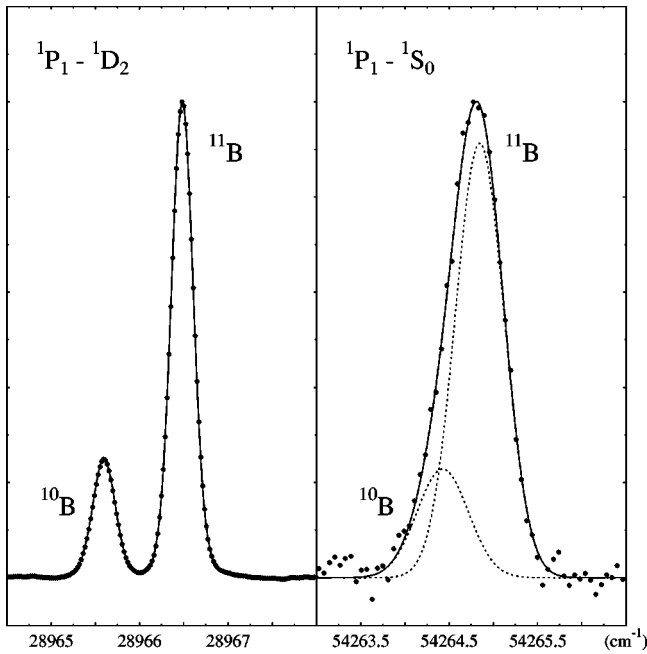


FIG. 2. FTS recording of the B II lines $2s2p\ ^1P_1 - 2p^2\ ^1D_2$ and $2s2p\ ^1P_1 - 2p^2\ ^1S_0$. The scale in cm^{-1} is the same in both parts of the figure. The solid and dotted lines show the profiles fitted to the observations, represented by the filled dots. The wave-number scale is not calibrated.

The interferometer was run at a resolution giving the instrumental linewidth $0.070\ \text{cm}^{-1}$. This is well below the expected Doppler width of boron lines emitted from a low-current hollow cathode discharge in the UV region, e.g., $0.25\ \text{cm}^{-1}$ at $2000\ \text{\AA}$ and the temperature $500\ \text{K}$. Two of the B II lines included in the present study were recorded with the FTS instrument, i.e., $2s2p\ ^1P_1 - 2p^2\ ^1D_2$ at $3451\ \text{\AA}$ and $2s2p\ ^1P_1 - 2p^2\ ^1S_0$ at $1842\ \text{\AA}$. The two isotope components from ^{10}B and ^{11}B are completely resolved at $3451\ \text{\AA}$, while the isotope effect in the $1842\text{-}\text{\AA}$ line only causes a slight asymmetry; see Fig. 2. This difference has two reasons: The transition isotope shift of the $3451\text{-}\text{\AA}$ line is twice as large as that of the $1842\text{-}\text{\AA}$ line (see below) and the Doppler width (on an energy scale) is larger at $1842\ \text{\AA}$ compared to $3451\ \text{\AA}$ by the factor $3451/1842=1.9$. The investigation of the boron spectrum with this equipment has been described previously by Kasten [7].

C. Data reduction and calibration

The wavelength of the $1362\text{-}\text{\AA}$ B II resonance line was determined from the photographic recordings with the $\text{B}_4\text{C}/\text{Fe}$ cathode. Highly accurate Fe II Ritz standards [8] were used as reference lines, providing a wavelength scale accurate to $0.0005\ \text{\AA}$. Short, low-current exposures were used, where the B II line showed no asymmetry, i.e., where the ^{10}B component was too weak to be detected and the recorded boron line was due to ^{11}B . The data reduction was performed by means of a package consisting of a computer-controlled scanning microdensitometer and a set of programs for peak finding and wavelength calibration [9]. The final result for the ^{11}B wavelength is $1362.460\ \text{\AA}$. The uncertainty is estimated as $\pm 0.001\ \text{\AA}$, which is larger than might be expected from the accuracy of the wavelength scale, but mo-

tivated by the fact that a small influence from the ^{10}B component cannot be completely excluded.

The ^{10}B , ^{11}B interval was determined from the photoelectric recordings by means of curve fitting routines. Gaussian line profiles were used and calculations were made with different combinations of free parameters: in addition to the line positions, also the linewidths and the intensity ratio. Consistent results were obtained, with the finally accepted value $13.0 \pm 0.5\ \text{m\AA}$.

For the $2s2p\ ^3P - 2p^2\ ^3P$ multiplet at $1624\ \text{\AA}$ both the wavelengths and the isotope shifts were determined from the photographic recording. Also in this case Fe II Ritz standards were used for the wavelength calibration, with a final wavelength uncertainty for the ^{11}B lines (excepting the weakest) of $1\ \text{m\AA}$.

The isotope intervals were determined by means of curve fitting to the microdensitometer recordings, but due to the nonlinear photographic response the uncertainty is larger, estimated as $4\ \text{m\AA}$ for the weakest line (low signal-to-noise ratio), $3\ \text{m\AA}$ for the strongest line (wide due to overexposure), and $2\ \text{m\AA}$ for the remaining four lines.

The data reduction of the FTS recordings was performed by means of the computer code DECOMP [11], where Voigt functions are fitted to the observed lines. Fe I and Fe II lines were used for the wave-number calibration [10]. The wave-number uncertainty of the completely resolved components of the $3451\text{-}\text{\AA}$ line (Fig. 2) is estimated as $0.002\ \text{cm}^{-1}$, which corresponds to $0.2\ \text{m\AA}$. The uncertainty of the $1842\text{-}\text{\AA}$ line, unresolved and having a lower S/N ratio, is larger. From a comparison of different fitting procedures with different sets of free parameters it is estimated as $0.02\ \text{cm}^{-1}$ or $1\ \text{m\AA}$ for both components.

III. EXPERIMENTAL RESULTS

The results of the measurements are shown in Table I. Wavelengths and wave numbers with estimated uncertainties are given for both isotopes. The table also contains the wavelength and wave-number differences of the isotopes, the transition isotope shifts. Since the relativistic effects are small in boron, all lines of an LS multiplet are expected to have the same TIS. Considering the uncertainties, this is seen in Table I to be the case for the $^3P\text{-}^3P$ multiplet, where the average value of the isotope shift is $19 \pm 1\ \text{m\AA}$ or $0.72 \pm 0.04\ \text{cm}^{-1}$.

The B II energy levels of the configurations $2s^2$, $2s2p$, and $2p^2$ in ^{10}B and ^{11}B derived from the observations are shown in Table II. The singlet energies are given relative to the ground state, which is set equal to zero for both isotopes. No intercombination lines have been observed in B II and the triplet levels of both isotopes are therefore given relative to the value $37\ 358.3\ \text{cm}^{-1}$ of $2s2p\ ^3P_2$ reported by Olme [12]. That value was derived during the analysis of the B II spectrum and based on the assumption that $2s6g\ ^1G$ and 3G coincide. The average value of the isotope shift $0.72\ \text{cm}^{-1}$ was used for all the lines of the $^3P\text{-}^3P$ multiplet.

The last column of the table shows the fine-structure intervals of the triplets. Reliable experimental values of these intervals are important for providing a check of the accuracy of different computational methods [13]. The table shows that the observed value of the $2s2p\ ^3P_2 - ^3P_0$ splitting is $22.26\ \text{cm}^{-1}$. The most recent calculations by Froese Fischer

TABLE I. Observed isotope structure of the $2s^2-2s2p$ and $2s2p-2p^2$ lines in B II.

Combination	^{10}B		^{11}B		TIS	
	λ (Å)	σ (cm^{-1})	λ (Å)	σ (cm^{-1})	$\Delta\lambda$ (mÅ)	$\Delta\sigma$ (cm^{-1})
$2s^2-2s2p$						
$^1S_0-^1P_1$	1362.473(1)	73 395.95(5)	1362.460(1)	73 396.65(5)	13	0.70
$2s2p-2p^2$						
$^3P_1-^3P_2$	1623.614(2)	61 590.99(8)	1623.593(1)	61 591.79(4)	21	0.80
$^3P_0-^3P_1$	1623.805(2)	61 583.75(8)	1623.786(1)	61 584.47(4)	19	0.72
$^3P_1-^3P_1$	1623.966(4)	61 577.64(15)	1623.947(2)	61 578.36(8)	18	0.72
$^3P_2-^3P_2$	1624.036(3)	61 574.99(11)	1624.020(1)	61 575.60(4)	16	0.61
$^3P_1-^3P_0$	1624.190(2)	61 569.15(8)	1624.171(1)	61 569.87(4)	19	0.72
$^3P_2-^3P_1$	1624.391(2)	61 561.53(8)	1624.372(1)	61 562.25(4)	19	0.72
$^1P_1-^1S_0$	1842.831(1)	54 264.337(20)	1842.817(1)	54 264.756(20)	14	0.419
$^1P_1-^1D_2$	3451.3876(2)	28 965.555(2)	3451.2819(2)	28 966.442(2)	105.7	0.887

and Gaigalas [14] and by Zhu and Chung [15] give, respectively, 22.19 cm^{-1} and 22.2 cm^{-1} , i.e., there is an excellent agreement between these calculations and the present observation.

IV. THEORY

The starting point for nonrelativistic atomic calculations is the zeroth-order Hamiltonian

$$H_0 = \sum_{i=1}^N \left(-\frac{\nabla_i^2}{2m} - \frac{Z}{r_i} \right) + \sum_{i<j}^N \frac{1}{r_{ij}}, \quad (1)$$

where the nucleus is assumed to be a point charge of infinite mass. When the effects of the finite nuclear mass and size are taken into account, the calculated energy levels are slightly shifted. Energy levels of different isotopes of an element are shifted differently, leading to the so-called level isotope shift. Taking the difference between the shifts for the upper and lower levels in a transition, the experimentally observable TIS is obtained.

In general, the atomic nucleus possesses higher-order electromagnetic moments, not included in the zeroth-order Hamiltonian, that interact with the electrons. The inclusion of these interactions leads to the hyperfine-structure splitting

TABLE II. Energy levels (cm^{-1}) of the B II configurations $2s^2$, $2s2p$, and $2p^2$. Singlet energies are relative to the ground state and triplet energies are relative to $2s2p \ ^3P_2 = 37\,358.30 \text{ cm}^{-1}$.

Designation	^{10}B	^{11}B	ΔE
$2s^2 \ ^1S_0$	0.00	0.00	
$2s2p \ ^3P_0$	37 336.04	37 336.04	
$2s2p \ ^3P_1$	37 342.15	37 342.15	6.11
$2s2p \ ^3P_2$	37 358.30	37 358.30	16.15
$2s2p \ ^1P_1$	73 395.95	73 396.65	
$2p^2 \ ^3P_0$	98 911.30	98 912.02	
$2p^2 \ ^3P_1$	98 919.79	98 920.51	8.49
$2p^2 \ ^3P_2$	98 933.18	98 933.90	13.39
$2p^2 \ ^1D_2$	102 361.51	102 363.09	
$2p^2 \ ^1S_0$	127 660.29	127 661.41	

of the calculated levels. All the above effects are small and can, to a very good approximation, be treated in first-order perturbation theory.

A. Isotope shift

For a finite nuclear mass M , the kinetic energy of the nucleus must be considered. Using the momentum conservation law in the center-of-mass coordinate system, the operator for the internal kinetic energy of an N -electron atom becomes [16]

$$H_{\text{kin}} = -\sum_{i=1}^N \frac{\nabla_i^2}{2\mu} - \frac{1}{M} \sum_{i<j}^N \nabla_i \cdot \nabla_j. \quad (2)$$

The first term includes a correction to the electron mass in which the mass m is replaced by the reduced mass $\mu = Mm/(M+m)$. This change in mass leads to an energy correction

$$E_{\text{NMS}} = E - E_0 = -E_0 \frac{m}{M+m}. \quad (3)$$

This is the normal mass shift. The inclusion of the second term leads to an additional energy correction known as the specific mass shift

$$E_{\text{SMS}} = E - E_0 = -\left\langle \psi \left| \frac{1}{M} \sum_{i<j}^N \nabla_i \cdot \nabla_j \right| \psi \right\rangle. \quad (4)$$

The specific mass shift is most conveniently expressed in terms of the specific mass shift parameter S ,

$$S = -\left\langle \psi \left| \sum_{i<j}^N \nabla_i \cdot \nabla_j \right| \psi \right\rangle, \quad (5)$$

which is the expectation value of the mass-independent factor of the specific mass shift operator.

Normally, also the shift due to the finite nuclear size (field shift) needs to be evaluated. For boron, however, this shift is negligible compared to the mass shift.

B. Hyperfine structure

The hyperfine structure of the atomic energy levels is caused by the interaction between the electrons and the electromagnetic multipole moments of the nucleus. The hyperfine interaction couples the nuclear and electronic angular momenta to a total momentum $\vec{F} = \vec{I} + \vec{J}$. The eigenfunction of the coupled state is $|\gamma I J F M_F\rangle$ and the energy corrections of the fine-structure level J are

$$W_{M1}(J) = \frac{1}{2} A_J C, \quad (6)$$

$$W_{E2}(J) = B_J \frac{\frac{3}{4} C(C+1) - I(I+1)J(J+1)}{2I(2I-1)J(2J-1)}, \quad (7)$$

where $C = F(F+1) - J(J+1) - I(I+1)$. Conventionally, the interaction constants A_J and B_J are given in MHz. To convert to cm^{-1} the conversion factor $1 \text{ MHz} = 3.335\,641\,0 \times 10^{-5} \text{ cm}^{-1}$ should be used.

C. Transition probabilities

The weighted oscillator strength, or gf value, for a transition between a term $\gamma' L' S'$ and a term $\gamma L S$ can be written in two forms, the length and velocity

$$gf_l = \frac{2}{3} \Delta E \left| \left\langle \gamma L S \left\| \sum_{i=1}^N r_i C^{(1)}(i) \right\| \gamma' L' S' \right\rangle \right|^2, \quad (8)$$

$$gf_v = \frac{2}{3} \Delta E^{-1} \left| \left\langle \gamma L S \left\| \sum_{i=1}^N \nabla^{(1)}(i) \right\| \gamma' L' S' \right\rangle \right|^2. \quad (9)$$

The two forms give the same results for exact wave functions. For approximate wave functions they will differ, and this can be used as a measure of the accuracy of the calculated values. Normally, at a given level of approximation, the length form is the preferred one. Also, this form shows the best convergence pattern as an approximate wave function is systematically improved.

V. METHOD OF CALCULATION

The wave functions were generated with the multiconfiguration Hartree-Fock (MCHF) atomic structure package of Froese Fischer [16], where the wave function ψ for a state labeled $\gamma L S$ is expanded in terms of configuration state functions (CSFs) with the same LS term

$$\psi(\gamma L S) = \sum_j c_j \Phi(\gamma_j L S). \quad (10)$$

In the numerical MCHF approach the CSFs are sums of products of spin orbitals, where the radial part of the spin orbital is represented by its numerical values at a number of grid points. In the multiconfigurational self-consistent field procedure both the orbitals and the expansion coefficients are optimized to self-consistency.

The calculations of the specific mass shift parameter and the hyperfine-structure constants from the MCHF wave functions were done with the isotope shift and hyperfine-structure

programs [17,18] that are part of the MCHF atomic structure package. The evaluation of the gf values between two separately optimized wave functions was done with a recently developed program based on the biorthonormal transformation technique [19].

The configuration expansions were obtained with the active space method, where CSFs of a particular parity and LS symmetry are generated by excitations from the reference configuration to an active set of orbitals. The active set is then increased in a systematic way, allowing the convergence of the calculated properties to be studied. If all possible excitations to the active set are allowed, the configuration-state expansion, referred to as the complete active space, grows very rapidly with the increasing active set. Many of these configurations, obtained mainly from three- and four-particle excitations, have very small expansion coefficients and contribute little to the total energy or to the studied parameters. By imposing different restrictions on the allowed excitations the number of configuration states can be kept down but with only a small change of the final results. In the present calculations only configurations where at least two of the orbitals had principal quantum numbers $n < 4$ were included. In addition, the active set was limited to include only s , p , d , and f orbitals. This limitation on the active set is believed to be unimportant for the specific mass shift, which, due to the orbital angular momentum restrictions on the one-particle matrix elements, is rather insensitive to orbitals with high angular momenta. A somewhat larger effect can be expected for the transition energies and oscillator strengths that are more slowly convergent with respect to the orbital angular momenta.

VI. THEORETICAL RESULTS

In Table III the total energies and specific mass shift parameters for $2s^2\,^1S$, $2s2p\,^3P$, $2s2p\,^1P$, $2p^2\,^3P$, $2p^2\,^1D$, and $2p^2\,^1S$ are shown as functions of the increasing active set of orbitals. The notation for the active set follows the conventions used in quantum chemistry. The set $3s2p1d$, for example, consists of three s , two p , and one d orbitals. From the table it is seen that the specific mass shift parameters, with the exception of the one for $2p^2\,^1S$, converge very well with respect to the increasing active set. The reason for the somewhat slow convergence for $2p^2\,^1S$ is not known, but may be related to the fact that this state is the second of the even-parity 1S symmetry. All the other states are the lowest of their symmetry.

Since the isotope shift in a transition is determined by the difference of the level isotope shift for the upper and lower levels, it is interesting to monitor the difference of the specific mass shift parameters for the two levels. In Table IV these differences are shown as functions of the increasing active set of orbitals. Although the individual specific mass shift parameters for the upper and lower states change very much with the increasing active set of orbitals, the differences are, with the exception for the $2s2p\,^1P - 2p^2\,^1S$ transition, comparatively constant and even rather small expansions give acceptable values. The $2s2p\,^1P - 2p^2\,^1S$ transition is interesting since it shows a different and much slower convergence pattern. In this case the active set needs to be increased further to obtain convergence at the subper-

TABLE III. Energies (E_0) and specific mass shift parameters (S) (a.u.) of the $2s^2$, $2s2p$, and $2p^2$ configurations in B II as functions of the increasing active set (AS) of orbitals.

AS	E_0	S	E_0	S	E_0	S
	$2s^2\ ^1S$		$2s2p\ ^3P$		$2s2p\ ^1P$	
$2s1p$	-24.296 413	-0.020 17	-24.120 378	-0.556 89	-23.913 062	-0.401 07
$3s2p1d$	-24.334 811	0.625 18	-24.163 773	0.107 87	-23.988 668	0.291 44
$4s3p2d1f$	-24.342 408	0.624 81	-24.171 729	0.110 03	-24.001 844	0.256 34
$5s4p3d2f$	-24.345 983	0.601 55	-24.175 638	0.090 27	-24.008 395	0.278 04
$6s5p4d3f$	-24.347 122	0.598 48	-24.177 088	0.088 81	-24.010 894	0.276 12
$7s6p5d4f$	-24.347 561	0.597 71	-24.177 627	0.088 04	-24.011 947	0.275 76
	$2p^2\ ^3P$		$2p^2\ ^1D$		$2p^2\ ^1S$	
$2s1p$	-23.849 576	-0.997 95	-23.793 976	-0.965 63		
$3s2p1d$	-23.881 092	-0.310 50	-23.860 636	-0.428 61	-23.729 892	0.342 43
$4s3p2d1f$	-23.889 943	-0.330 73	-23.871 971	-0.430 23	-23.755 310	0.160 04
$5s4p3d2f$	-23.895 190	-0.315 46	-23.878 139	-0.403 10	-23.761 323	0.157 73
$6s5p4d3f$	-23.896 691	-0.318 10	-23.879 997	-0.406 46	-23.763 731	0.137 91
$7s6p5d4f$	-23.897 204	-0.318 91	-23.880 826	-0.407 05	-23.764 670	0.131 42

cent level. Looking at the transition energies, these are in good agreement with experiment for $2s2p\ ^3P-2p^2\ ^3P$ and $2s2p\ ^1P-2p^2\ ^1S$. For the remaining two transitions the difference is of the order 200 cm^{-1} . The major part of this difference can be attributed to the absence of orbitals with high orbital angular momenta in the active set.

In Table IV also the gf values are shown in the length and velocity forms. For the $2s^2\ ^1S-2s2p\ ^1P$ and $2s2p\ ^3P-2p^2\ ^3P$ transitions the agreement between the length and the velocity forms is very good and the values agree to within one part in 1000 with the values from the benchmark calculations by Weiss [20] and by Godefroid *et al.* [21]. For the $2s2p\ ^1P-2p^2\ ^1D$ and $2s2p\ ^1P-2p^2\ ^1S$ transitions, however, the two forms of the gf values differ by between 1% and 2%, indicating that important

correlation effects have been left out. These effects are most likely described by orbitals with high orbital angular momenta, i.e., g , h , and i orbitals. Clearly, if a subpercent accuracy is targeted the latter orbitals need to be included in the active set. This, however, leads to larger configuration expansions and an increasing use of CPU time. For the $2s2p\ ^1P-2p^2\ ^1D$ transition the difference between the present gf value in the length form and the supposedly more accurate value of Weiss is 2%. For $2s2p\ ^1P-2p^2\ ^1S$ the difference is less than three parts in 1000. The theoretical gf values for the $2s^2\ ^1S-2s2p\ ^1P$, $2s2p\ ^3P-2p^2\ ^3P$, and $2s2p\ ^1P-2p^2\ ^1S$ transitions are all within the error bars of the beam-foil measurements by Bashkin *et al.* [22].

From the parameters in Table IV the $^{11}\text{B}-^{10}\text{B}$ transition isotope shifts were calculated. The shifts are presented in

TABLE IV. Transition energies (cm^{-1}), differences of the specific mass shift parameters (a.u.), and gf values in the length and velocity forms for the $2s^2-2s2p$ and $2s2p-2p^2$ transitions in B II as functions of the AS of orbitals.

AS	ΔE	ΔS	gf_l	gf_v	ΔE	ΔS	gf_l	gf_v
	$2s^2\ ^1S-2s2p\ ^1P$				$2s2p\ ^3P-2p^2\ ^3P$			
$2s1p$	84 132	-0.380 90	1.0652	0.7914	59 431	-0.441 07	3.3646	2.6045
$3s2p1d$	75 966	-0.333 74	1.0216	0.9939	62 038	-0.418 37	3.1366	3.3046
$4s3p2d1f$	74 742	-0.368 44	1.0186	1.0258	61 842	-0.440 76	3.1157	3.1136
$5s4p3d2f$	74 088	-0.323 51	1.0053	1.0036	61 548	-0.405 73	3.0859	3.1021
$6s5p4d3f$	73 790	-0.322 36	1.0020	1.0004	61 537	-0.406 91	3.0829	3.0890
$7s6p5d4f$	73 655	-0.321 94	1.0011	0.9999	61 543	-0.406 95	3.0828	3.0840
Expt.	73 397				61 577			
	$2s2p\ ^1P-2p^2\ ^1D$				$2s2p\ ^1P-2p^2\ ^1S$			
$2s1p$	26 135	-0.564 56	0.8676	0.3180				
$3s2p1d$	28 098	-0.720 05	0.4658	0.4011	56 792	0.050 98	0.618 53	0.659 59
$4s3p2d1f$	28 502	-0.686 57	0.4870	0.4777	54 105	-0.096 30	0.666 56	0.691 76
$5s4p3d2f$	28 586	-0.681 13	0.4819	0.4783	54 223	-0.120 31	0.670 48	0.689 69
$6s5p4d3f$	28 727	-0.682 58	0.4804	0.4690	54 243	-0.138 20	0.675 68	0.685 70
$7s6p5d4f$	28 776	-0.682 81	0.4792	0.4705	54 268	-0.144 34	0.677 15	0.684 74
Expt.	28 965				54 265			

TABLE V. Calculated isotope shifts $\Delta\sigma$ (cm^{-1}) and $\Delta\lambda$ ($\text{m}\text{\AA}$) of the $2s^2$ - $2s2p$ and $2s2p$ - $2p^2$ transitions in B II.

Combination	$\Delta\sigma_{\text{NMS}}$	$\Delta\sigma_{\text{SMS}}$	$\Delta\sigma_{\text{tot}}$	$\Delta\lambda_{\text{tot}}$
$2s^2$ - $2s2p$				
1S - 1P	0.3640	0.3505	0.7145	13.27
$2s2p$ - $2p^2$				
3P - 3P	0.3054	0.4431	0.7485	19.74
1P - 1S	0.2692	0.1571	0.4263	14.48
1P - 1D	0.1437	0.7433	0.8870	105.8

Table V, which shows that the experimental and the theoretical TISs agree within the error limits. Good agreement between theoretical and experimental values has been found previously for a number of other transitions in more complex atoms [23,24].

Both ^{11}B and ^{10}B have a nonzero nuclear spin leading to a hyperfine-structure splitting of the fine-structure levels belonging to $2s2p$ 3P , $2s2p$ 1P , $2p^2$ 3P , and $2p^2$ 1D . The corresponding hyperfine-structure constants are shown in Table VI. These constants are believed to be correct to within 1% or 2%, with the exception of A_2 for $2p^2$ 3P_2 , which is rather uncertain due to large cancellation effects. From the interaction constants the energy splitting between the outmost hyperfine-structure components, corresponding to $F=I+J$ and $F=|I-J|$, can be calculated. The splittings for $2s2p$ 3P_1 and $2s2p$ 3P_2 , the most prominent cases, in ^{11}B are 0.123 cm^{-1} and 0.199 cm^{-1} , respectively.

In an effort to establish the $2s3s$ 1S level, calculations were also performed for the $2s2p$ 1P - $2s3s$ 1S transition. These calculations predicted a transition energy of $64\,125 \text{ cm}^{-1}$ or 1559.45 \AA . The gf value for this line, due to large cancellations in the transition matrix element, was found to be very small (see also Ref. [20]). An experimental value for the $2s3s$ 1S level was reported by Ölme [12], who identified a line at 1607.76 \AA as $2s2p$ 1P - $2s3s$ 1S . Ölme's value was revised by Bashkin *et al.* [22], who derived a value for $2s3s$ 1S from a line at 2014.1 \AA , identified as a transition from $2p3s$ 1P . This predicts the $2s2p$ 1P - $2s3s$ 1S line to appear at 1573 \AA , not confirmed by Bashkin *et al.* due to a blend at their low-resolution beam-foil recording. It has not been possible to find any line around 1573 \AA in the present work, positively identified as B II and thus confirming the prediction by Bashkin *et al.* Neither was it possible to find any line supporting the theoretical prediction 1559.45 \AA . The difficulty to find the line may be explained by the predicted low gf value, but the lack of agreement between the theo-

TABLE VI. Calculated hyperfine interaction constants (in MHz) for the $2s2p$ and $2p^2$ states in ^{11}B (the corresponding values for ^{10}B can be obtained by scalings with, respectively, $\mu_{^{10}\text{B}}I_{^{11}\text{B}}/\mu_{^{11}\text{B}}I_{^{10}\text{B}}=0.3349$ and $Q_{^{10}\text{B}}I_{^{11}\text{B}}/Q_{^{11}\text{B}}I_{^{10}\text{B}}=2.084$).

Designation	A_1	A_2	B_1	B_2
$2s2p$ 3P	918.80	794.05	-2.089	4.178
$2s2p$ 1P	181.40		3.835	
$2p^2$ 3P	-112.60	10.90	2.081	-4.163
$2p^2$ 1D		178.99		7.692

retically predicted wavelength and that derived from the observations of Bashkin implies that the position of $2s3s$ 1S is still an unresolved problem.

VII. SUMMARY AND CONCLUSIONS

We report on accurate grating and FTS measurements of wavelengths and isotope shifts for the LS -allowed $2s^2$ - $2s2p$ and $2s2p$ - $2p^2$ transitions in B II. The measurements are supported by large-scale multiconfiguration Hartree-Fock calculations, which, in addition to the isotope shifts, also give the oscillator strengths and the hyperfine structures. The experimental and theoretical isotope shifts are in agreement within the error limits.

To check the proposed cosmic production processes of the light elements, it is important to determine the relative abundance of ^{10}B and ^{11}B in various stellar objects. Due to the small isotope shift the spectral lines from the two isotopes cannot be resolved. Instead, the abundance determination needs to be done through curve fitting to asymmetric line profiles. The present data provide the basis for such a fitting and should therefore be of great astrophysical interest.

ACKNOWLEDGMENTS

Financial support by the Swedish Natural Science Research Council (NFR), the Swedish National Space Board (DFR), and the Deutsche Forschungsgemeinschaft (DFG) is gratefully acknowledged. The authors are indebted to Maurice Benharrous for his assistance in the Meudon measurements. Computer resources were made available by C. Froese Fischer at Vanderbilt University through a grant from the Division of Chemical Sciences, Office of Basic Energy Sciences, Office of Energy Research, U.S. Department of Energy.

- [1] S.R. Federman, D.L. Lambert, J.A. Cardelli, and Y. Sheffer, *Nature (London)* **381**, 764 (1996).
 [2] T. Zethson *et al.* (unpublished).
 [3] S.G. Johansson, U. Litzén, J. Kasten, and M. Kock, *Astrophys. J.* **403**, L25 (1993).
 [4] P. Jönsson, S.G. Johansson, and C. Froese Fischer, *Astrophys. J.* **429**, L45 (1994).

- [5] K. Danzmann, M. Günther, J. Fischer, M. Kock, and M. Kühne, *Appl. Opt.* **27**, 4947 (1988).
 [6] A.P. Thorne, C.J. Harris, I. Wynne-Jones, R.C.M. Learner, and G. Cox, *J. Phys. E* **20**, 54 (1987).
 [7] J. Kasten, Ph.D.thesis, Universität Hannover, 1992 (unpublished).
 [8] G. Nave, S. Johansson, and A. Thorne, *J. Opt. Soc. Am. B* **14**,

- 1035 (1997).
- [9] B. Skogvall, Lund University, Department of Physics, LRAP 58, 1986 (unpublished).
- [10] G. Nave, R.C.M. Learner, A.P. Thorne, and C.J. Harris, *J. Opt. Soc. Am. B* **8**, 2028 (1991).
- [11] J.W. Brault and M.C. Abrams, *OSA Technical Digest Series* (Optical Society of America, Washington, DC, 1989), Vol. 6, p. 110.
- [12] A. Ölme, *Phys. Scr.* **1**, 256 (1970).
- [13] T. Brage, J. Fleming, and R. Hutton (unpublished).
- [14] C. Froese Fischer and G. Gaigalas, *Phys. Scr.* **56**, 436 (1997).
- [15] X.-W. Zhu and K.T. Chung, *Phys. Rev. A* **50**, 3818 (1994).
- [16] C. Froese Fischer, T. Brage, and P. Jönsson, *Computational Atomic Structure, An MCHF Approach* (Institute of Physics, Bristol, 1997).
- [17] P. Jönsson and C. Froese Fischer, U.S. Department of Energy Technical Report No. DOE/ER/13867-14, 1994 (unpublished).
- [18] P. Jönsson, C.-G. Wahlström, and C. Froese Fischer, *Comput. Phys. Commun.* **64**, 369 (1991).
- [19] J. Olsen, M. Godefroid, P. Jönsson, P.-Å. Malmqvist, and C. Froese Fischer, *Phys. Rev. E* **52**, 4499 (1995).
- [20] A.W. Weiss, *Phys. Rev. A* **51**, 1067 (1995).
- [21] M. Godefroid, J. Olsen, P. Jönsson, and C. Froese Fischer, *Astrophys. J.* **450**, 473 (1995).
- [22] S. Bashkin, L.C. McIntyre, H.v. Buttlar, J.O. Ekberg, and I. Martinson, *Nucl. Instrum. Methods Phys. Res. B* **9**, 593 (1985).
- [23] P. Jönsson and C. Froese Fischer, *Phys. Rev. A* **30**, 3080 (1994).
- [24] J. Carlsson, P. Jönsson, M.R. Godefroid, and C. Froese Fischer, *J. Phys. B* **28**, 3729 (1995).